Solar wind impacts on growth phase duration and substorm intensity: A statistical approach

H. Li,[1] C. Wang,[1] and Z. Peng[1]

Received 14 March 2013; revised 22 May 2013; accepted 16 June 2013; published 23 July 2013.

[1] A statistical survey of 379 interplanetary magnetic field (IMF) southward turning events during the time period from 1995 to 2011 is performed to study the impact of solar wind conditions on the substorm growth phase duration and intensity. Substorm growth phase persists from several minutes up to 2–3 h, and its duration is mainly controlled by solar wind conditions. The larger dayside reconnection E-field and solar wind speed are, the shorter the growth phase will be. The lower limits of solar wind reconnection E-field and bulk speed for substorm occurrence are found to be 0.6 mV/m and 280 km/s, respectively. Similarly, the substorm intensity is linearly correlated to the dayside reconnection E-field. However, it seems to be independent of the amount of dayside geomagnetic flux reconnected and solar wind energy entered into the magnetosphere during the growth phase. Furthermore, all the events are divided into three groups for different averages of dayside reconnection E-field during the growth phase ($\overline{E_{\mathrm{KL}}}$): (1) $0.0 \leq \overline{E_{\mathrm{KL}}} < 1.5$ mV/m; (2) $1.5 \leq \overline{E_{\mathrm{KL}}} < 2.5$ mV/m; and (3) $\overline{E_{\mathrm{KL}}} \geq 2.5$ mV/m, and the geometric means of growth phase duration and auroral power maximum for these three groups are 91 min, 62 min, 32 min, and 35 GW, 51 GW, 74 GW, respectively.

Citation: Li, H., C. Wang, and Z. Peng (2013), Solar wind impacts on growth phase duration and substorm intensity: A statistical approach, *J. Geophys. Res. Space Physics*, *118*, 4270–4278, doi:10.1002/jgra.50399.

1. Introduction

[2] *Akasofu* [1964] established the phenomenological auroral substorm model on the basis of abundant long-term auroral pictures obtained by ground-based all-sky cameras. *McPherron* [1970] thereafter realized that many different phenomena precede the actual substorm expansion onset, and introduced a growth phase prior to the expansion phase, during which the excess energy is stored in the magnetotail, and plasma sheet is reconfigured toward a more stretched state. It has been widely accepted that a gradual intensification of the eastward and westward auroral electrojets is associated with the growth phase caused by enhancements of the ionospheric convection electric field [*Kamide and Vickrey*, 1983].

[3] The magnetospheric changes during substorm growth phase are directly driven phenomena and, simultaneously, they are the part of the loading-unloading substorm sequence [*Rostoker*, 1969]. Directly driven process leads to a dominant two-cell DP-2 current system in high-latitude ionosphere during growth phase [*Kamide and Fukushima*, 1972], while loading-unloading process leads to a dominant one-cell DP-1 current system during expansion phase [*Akasofu et al.*, 1966].

[4] It has been widely accepted that IMF B_Z controls the energy input into the magnetosphere. And the substorm sequence is suggested to start when the interplanetary magnetic field (IMF) turns southward and activates the dayside magnetic reconnection [*Baker et al.*, 1984; *Baker*, 1996; *Russell and McPherron*, 1973]. After the IMF southward turning, the entire polar ionosphere normally responds within 2 min [*Ridley et al.*, 1997, 1998; *Ruohoniemi and Greenwald*, 1998] or at latest, after 15 min [*Cowley and Lockwood*, 1992]. Generally, substorm growth phase is determined to start with the abrupt IMF southward turning and end at the onset of optical auroral expansion phase [e.g., *Petrukovich*, 2000; *Tanskanen et al.*, 2002; *Gjerloev et al.*, 2003]. This phase has been shown to last some tens of minutes by many investigations. Usually, it is in the range of 20–160 min, with the average of $\sim$ 71 min [e.g.,*Foster et al.*, 1971; *Iijima and Nagata*, 1972; *Caan et al.*, 1977; *Iyemori*, 1980; *McPherron*, 1994; *Kamide and Kokubun*, 1996].

[5] Although many studies on substorm have been done in the past several decades, some important problems remain unsolved. For example, (1) the physical meaning of growth phase duration: *Rostoker et al.* [1972] suggested that growth phase duration is governed by the amount of energy stored in the magnetosphere, while *Meng et al.* [1973] interpreted the duration to be mainly caused by the difference in the durations of southward IMF B_Z; (2) the relationship of growth phase duration to solar wind conditions: *Dmitrieva and Sergeev* [1983, 1985] and *Petrukovich* [2000] found that

[1] State Key Laboratory of Space Weather, Center for Space Science and Applied Research, Chinese Academy of Sciences, Beijing, China.

Corresponding author: H. Li, State Key Laboratory of Space Weather, Center for Space Science and Applied Research, Chinese Academy of Sciences, P.O. Box 8701, Beijing 100190, China. (hli@spaceweather.ac.cn)

2169-9380/13/10.1002/jgra.50399

growth phase duration was inversely proportional to southward IMF B_Z, while *Iyemori* [1980] suggested that it had little dependence on southward IMF B_Z and selected a value of 60 min for the growth phase duration except for a few cases; (3) substorm occurrence rate: *Kamide et al.* [1977] argued that the occurrence probability of substorms were dependent on the intensity of IMF B_Z, while *Saito et al.* [1976] showed that a substorm could occur when the stored magnetotail lobe energy was still at a low level; (4) which solar wind parameter controls the substorm intensity: There are many parameters used in the literature as a gauge for the substorm intensity, including measurable quantities in the ionosphere, the magnetosphere, or a combination of these regions [e.g., see *Lui*, 1993, for a review]. So far, it is still an open issue as to which is the best measure of the substorm intensity. Furthermore, an important fundamental question as to what controls the substorm intensity is still unresolved. Nevertheless, many efforts have been made to explore the relationships between solar wind conditions and the substorm intensity. *Tanskanen et al.* [2005] proposed that the solar wind high-speed streams strongly modulate the substorm occurrence rate, peak amplitude, and ionospheric dissipation in the form of Joule heating and auroral electron precipitation. They found that the total ionospheric dissipation during a substorm is strongly correlated with high-speed solar wind stream activity. *Newell et al.* [2007] proposed a nearly universal solar wind-magnetosphere coupling function ($d\Phi/dt$) inferred from 10 magnetospheric state variables, finding that the correlation coefficient between $d\Phi/dt$ and AL index is –0.528. *Milan et al.* [2009] later concluded that the substorm intensity is governed by the open flux content of the magnetosphere, and substorms are more intense in terms of auroral brightness when the amount of open flux in the magnetosphere prior to expansion onset is larger.

[6] In an attempt to answer part of the above mentioned questions, we make a comprehensive statistical investigation of IMF southward turning events, focusing on the following two questions: (1) solar wind impacts on substorm growth phase duration; and (2) solar wind impacts on substorm intensity. This paper is organized as follows: The methodology is presented in section 2; the results are given in section 3; the discussion and summary are presented in sections 4 and 5, respectively.

2. Methodology

2.1. Identifying the List of IMF Southward Turning Event

[7] IMF southward turning events are identified by an auto-search computer program on the basis of 1 min OMNI data sets during the period from 1995 to 2011. The OMNI data sets combined solar wind plasma and interplanetary magnetic field data and have subtracted the time delay from upstream solar wind to the Earth's bow shock nose. The onset of IMF southward turning is remarked as T_{NS}. The selection criteria of an IMF southward turning event are listed as follows:

[8] 1. the upstream (1 h interval before T_{NS}) IMF should be mostly (> 85%) northward with the average value of B_Z greater than 1.0 nT;

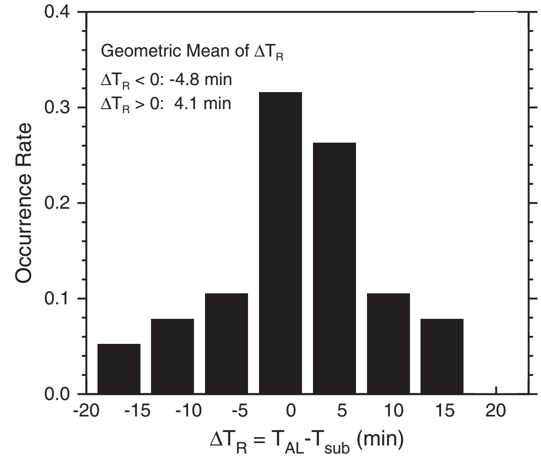

Figure 1. Distribution of time differences between T_{AL} (approximation of substorm onset by the beginning of the sudden sharp decrease of AL index after IMF southward turning) and T_{sub} (substorm onset identified from FUN images on board IMAGE satellite by *Frey et al.* [2004]).

[9] 2. the downstream (1 h interval after T_{NS}) IMF should be mostly (> 85%) southward with the average value of B_Z less than –1.0 nT;

[10] 3. the fluctuations of IMF B_Z for both upstream and downstream should be nonsignificant, with the ratio of standard deviation and average value less than 0.5;

[11] 4. the associated change of solar wind dynamic pressure should be very small (< 30%) to exclude the impact of dynamic pressure changes on substorm expansion onset;

[12] 5. no substorm occurs during the upstream period (the mean AL index is greater than –100 nT and without any clear fluctuations);

[13] 6. associated with a sudden decrease of AL index within the next 3 h after T_{NS}.

[14] Note that the duration of upstream and downstream is just used for identifying the IMF southward turning event. For practice, 1 h duration is used here. A longer duration, 2 h, is also tested. It only reduces the number of IMF southward turning events, but does not impact the following statistical analysis and main results. Through the above judgments, a total of 379 IMF southward turning events are identified during the concerned 17 years.

2.2. Determining the Duration of Substorm Growth Phase

[15] For investigating the solar wind impacts on growth phase duration and substorm intensity, both the growth phase duration and substorm intensity should be quantitatively determined first.

[16] The exact definition of growth phase onset can only be obtained synthetically based on measurements, e.g., IMF southward turning, global auroral images, decrease in AL index, increase in polar cap area, development of the geomagnetic DP-2 current system centered at the near-auroral oval region, enhancement of the tail current and/or the asymmetric ring current, etc. However, for simplicity, the onset of substorm growth phase was determined as the moment of IMF southward turning, remarking as T_{NS} [*Petrukovich*, 2000; *Tanskanen et al.*, 2002; *Gjerloev et al.*, 2003].

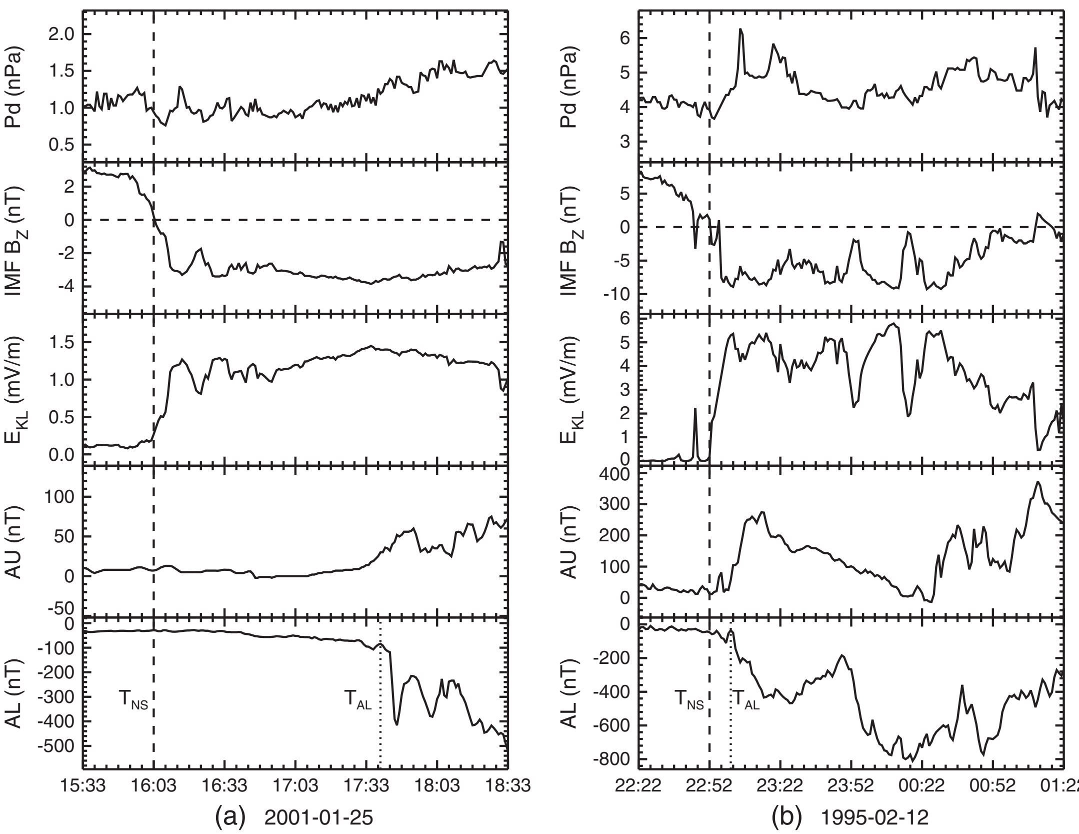

Figure 2. Two comparative events: (a) long-duration growth phase event on 25 January 2001; (b) short-duration growth phase event on 12 February 1995. From top to bottom, the panels give the solar wind dynamic pressure, IMF B_Z, solar wind electric field proposed by *Kan and Lee* [1979] E_{KL}, AU index, and AL index. The vertical dashed line remarks the onset of IMF southward turning (T_{NS}), and the vertical dotted line gives the onset of sudden AL decrease (T_{AL}).

[17] To determine the exact substorm expansion onset, a good direct approach is to use the continuous aurora observation with a high time resolution from auroral imaged either on-board polar-orbit satellites or equipped in the ground network. However, continuous aurora images are not available for most of the IMF southward turning events. *Hsu and McPherron* [1996, 1998] proposed an approximate selection of expansion onset by using both sharp AL decrease and Pi-2 wave burst. Similarly, we approximately estimate the expansion onset to be the beginning of the sudden sharp decrease of AL index after IMF southward turning, remarking as T_{AL}. In order to reduce the uncertainty in the data base, the AL index is required to drop to less than –100 nT within 1.5 h after its initial sudden decrease. Because there is no unique maximum level of AL index that could be qualified as a substorm, the threshold of –100 nT is, of course, an arbitrary choice to generally identify the event to be a substorm. Thus, the substorm event in the present study reaches less than –100 nT in AL index, and some very weak events are excluded. Similar treatments can also be found in *Tanskanen et al.* [2002].

[18] To test the validity of the above approximation of substorm expansion onset, a comparison of T_{AL} to auroral substorm onset (T_{sub}) identified from direct auroral observations is made. *Frey et al.* [2004] determined the auroral substorm onsets from auroral images by Far Ultraviolet Imaged (FUV) on board the IMAGE satellite from 19 May 2000 through 31 December 2002. During this time interval, there are 42 identified IMF southward turning events. The distribution of time differences (ΔT_R) between T_{AL} and T_{sub} is shown in Figure 1. For most of the events (58%), the time difference is less than 5 min. The geometric mean of ΔT_R is –4.8 min and 4.1 minutes for $\Delta T_R < 0$ and $\Delta T_R > 0$, respectively. The relative error ($|\Delta T_R/T_{\mathrm{AL}}|$) is very small, only about 5%. Thus, our approximation of substorm expansion onset is believed to be reasonable.

[19] After determining the onsets of growth phase (T_{NS}) and expansion phase (T_{AL}), the duration of substorm growth phase can be directly obtained from the time difference of these two onsets approximately, $\Delta T = T_{\mathrm{AL}} - T_{\mathrm{NS}}$. The error of growth phase duration estimation comes from both determining T_{NS} and T_{AL}. When determining T_{NS}, the error is on the order of several minutes from shifting the solar wind plasma and IMF data to account for the time delay from upstream observation to the Earth's bow shock nose. When determining T_{AL}, the error is about 4–5 min as shown in Figure 1. Thus, the error of growth phase duration is on the order of several minutes. Considering that the average value of growth phase duration is about 70 min based on previous studies, this error is acceptable, and it is still reliable for the statistical investigation of extreme large number of events.

2.3. Determining the Substorm Intensity

[20] The substorm intensity is relatively difficult to be determined. A proxy parameter is often used. Many parameters are used in the literature as a gauge for the substorm intensity, including measurable quantities in the ionosphere, the magnetosphere, or a combination of these regions [e.g., see *Lui*, 1993, for a review]. In terms of ionospheric quantities, there are auroral electrojet indices (AE and AL indices), the total current of the westward auroral electrojet, the total area of bright aurora in the polar region, the auroral power, the maximum poleward advance of the auroral bulge, and the duration of auroral substorm. In terms of magnetospheric quantities, the innermost location of the substorm injection boundary and the amount of cross-tail current reduction are used. The measure reflecting the substorm strength in both the ionosphere and the magnetosphere is the total energy dissipation during a substorm.

[21] Here we choose the maximum of hemispheric auroral power within 1.5 h after substorm expansion onset to represent the substorm intensity. The hemispheric auroral power data is provided by the Total Energy Detector (TED) instrument on board the NOAA/POES (formerly TIROS) series of polar orbiting satellites. The TED is designed to monitor the power flux carried into the Earth's atmosphere by precipitating auroral charged particles with energy from 50 eV to 20 keV. The POES satellites pass over the polar auroral regions twice each orbit, and make nearly polar orbits roughly 14.1 times a day. Concurrently in orbit, there is a morning and afternoon POES satellite, which can provide a continuous monitor of the auroral power flux.

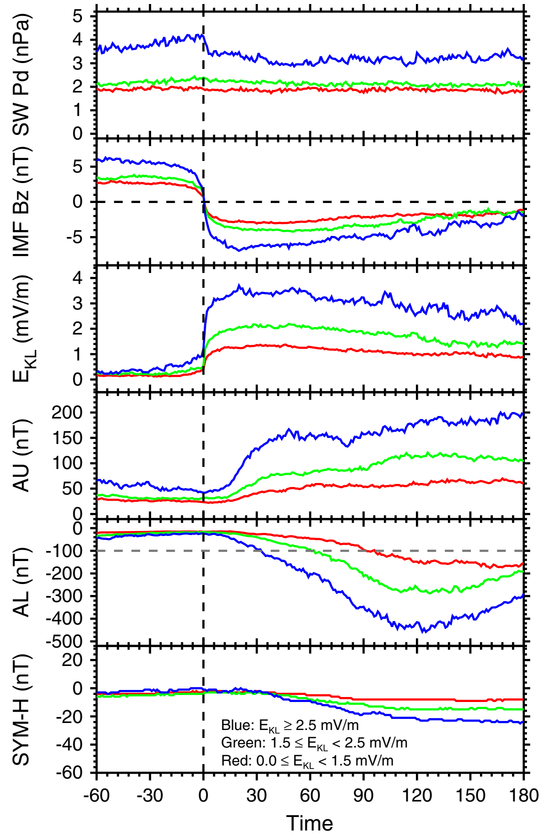

Figure 3. Results of the superposed epoch study for the IMF southward turning events. The onset of IMF southward turning is chosen to be the zero-epoch time as marked by the black vertical dashed line. From top to bottom, the panels give the medians of the solar wind dynamic pressure, the IMF B_Z, E_{KL}, AU index, AL index, and SYM-H index. The lines in red represent the first group of $0.0 \leq \overline{E_{KL}} < 1.5$ mV/m; the lines in green represent the second group of $1.5 \leq \overline{E_{KL}} < 2.5$ mV/m; and the lines in blue represent the third group of $\overline{E_{KL}} \geq 2.5$ mV/m.

3. Results

3.1. Long-Duration Growth Phase Event

[22] Figure 2a shows a long-duration growth phase event on 25 January 2001. From top to bottom, the panels give the solar wind dynamic pressure, IMF B_Z, solar wind electric field proposed by *Kan and Lee* [1979] E_{KL}, AU index, and AL index, respectively. The onset of IMF southward turning marked by the vertical dashed line is at 1603 UT, and the onset of sudden AL decrease marked by the vertical dotted line is at 1739 UT. The duration of growth phase is about 96 min. For this event, the IMF B_Z turns southward from 2.5 nT to –3.2 nT and remains southward for more than 2.5 h. Accordingly, the E_{KL} increases from 0.1 mV/m to about 1.0 mV/m. After the southward turning of IMF, the solar wind dynamic pressure varies nonsignificantly and remains about 1.0 nPa. Moreover, the AL index starts to decrease gradually from –29 nT to –107 nT, which is a well-known growth phase phenomenon. At the same time, the AU index remains invariant of about 10 nT. After the substorm expansion onset at 1739 UT, the AL index suddenly decreases to less than –500 nT within 1 h.

3.2. Short-Duration Growth Phase Event

[23] For comparison, Figure 2b shows a short-duration growth phase event on 12 February 1995. The onset of IMF southward turning is at 2252 UT, and the onset of sudden AL decrease is at 2301 UT. The duration of growth phase is only about 9 min. For this event, the IMF B_Z turns southward from 7.0 nT to –8.0 nT and remains southward for more than 2.0 h. Accordingly, the E_{KL} increases from 0.1 mV/m to about 5.0 mV/m. After the southward turning of IMF, the solar wind dynamic pressure has a weak enhancement (from 4.0 nPa to 5.0 nPa, increasing by about 25%), meanwhile, the AL index starts to decrease gradually from –47 nT to –111 nT. At the same time, the AU index decreases slowly from 12 nT to 81 nT. After the substorm expansion onset at 2301 UT, the AL index suddenly decreases to –434 nT within half an hour.

3.3. Superposed Epoch Analysis

[24] The above two typical events suggest that the duration of growth phase and substorm intensity seem to be correlated to the averaged value of solar wind electric field during the growth phase, $\overline{E_{KL}}$. To do further confirmation, we divided all the events into three groups according to different $\overline{E_{KL}}$ and performed a superposed epoch analysis of IMF southward turning events. The first group of $0.0 \leq \overline{E_{KL}} < 1.5$ mV/m contains 128 events; the second group of $1.5 \leq \overline{E_{KL}} < 2.5$ mV/m contains 151 events; and the third

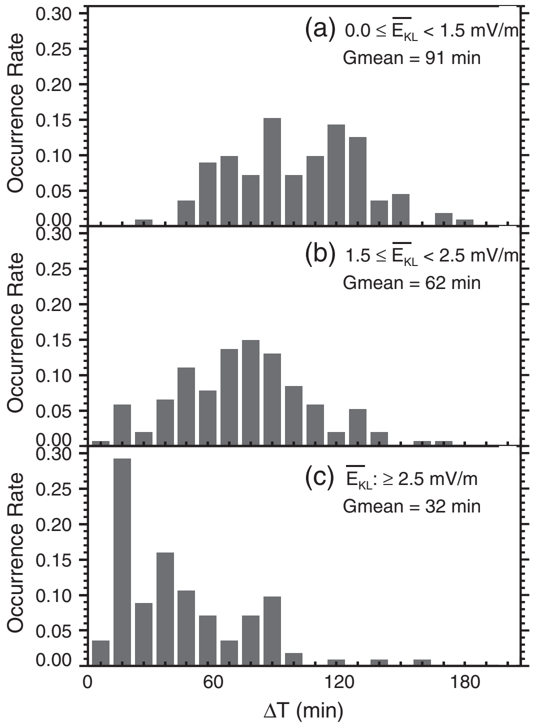

Figure 4. Histogram distribution of growth phase duration for every 10 min. (a–c) The three groups mentioned in section 3.3. The vertical coordinate represents the occurrence rate.

group of $\overline{E_{KL}} \geq 2.5$ mV/m contains 100 events. Each group contains enough cases for performing the superposed epoch analysis and maintaining statistical significance.

[25] Figure 3 shows the results of the superposed epoch study for the IMF southward turning events. The onset of IMF southward turning is chosen to be the zero-epoch time as marked by the black vertical dashed line. From top to bottom, the panels give the medians of the solar wind dynamic pressure, IMF B_Z, E_{KL}, AU index, AL index, and SYM-H index, respectively. There are no significant variations of solar wind dynamic pressure for each group seen as required by the selection criteria of IMF southward turning event. The downstream IMF B_Z after its southward turning for the three groups are –3.0 nT, –4.0 nT, and –6.5 nT, respectively. At the same time, the downstream E_{KL} are 1.2 mV/m, 2.2 mV/m, and 3.5 mV/m, respectively. The responses of AU index to the IMF southward turning are nearly at the same time for the three groups, about 10 min after IMF turning southward. However, the amplitudes of the AU enhancements are different, of 50 nT, 80 nT, and 150 nT, respectively. The responses of AL index are different for the three groups. The larger the downstream E_{KL} is, the earlier response of AL index occurs and the less minimum the AL index reaches. When the AL index decreases to –100 nT as marked by the gray dashed horizontal line, it is about 30 min, 60 min, and 90 min after IMF turning southward, respectively. Meanwhile, the minimum of AL index are about –160 nT, –260 nT and –450 nT, respectively.

3.4. Growth Phase Duration

[26] The histogram distribution of the growth phase duration for every 10 min is shown in Figure 4. Figure 4a–4c correspond to the three groups mentioned in section 3.3. The vertical axis represents the occurrence rate. It is clear that the distribution of growth phase duration moves leftward as the $\overline{E_{KL}}$ increases. For the group of $0.0 \leq \overline{E_{KL}} < 1.5$ mV/m, the duration of growth phase ranges mainly from 50 to 150 min, peaking at 90 min. The geometric mean is 91 min. For the group of $1.5 \leq \overline{E_{KL}} < 2.5$ mV/m, the duration of growth phase ranges mainly from 20 to 140 min, peaking at 80 min. The geometric mean decreases to 62 min. For the group of $\overline{E_{KL}} \geq 2.5$ mV/m, the duration of growth phase ranges mainly from 10 to 100 min, peaking at about 20 min. The geometric mean is only 32 min. The geometric means of growth phase duration for these three groups also match the results argued in the previous superposed epoch analysis.

[27] Figure 5 shows the impact of solar wind parameters on the growth phase duration. Figure 5 (left) The averaged value of solar wind electric field during the growth phase, $\overline{E_{KL}}$; Figure 5 (right) The averaged value of solar

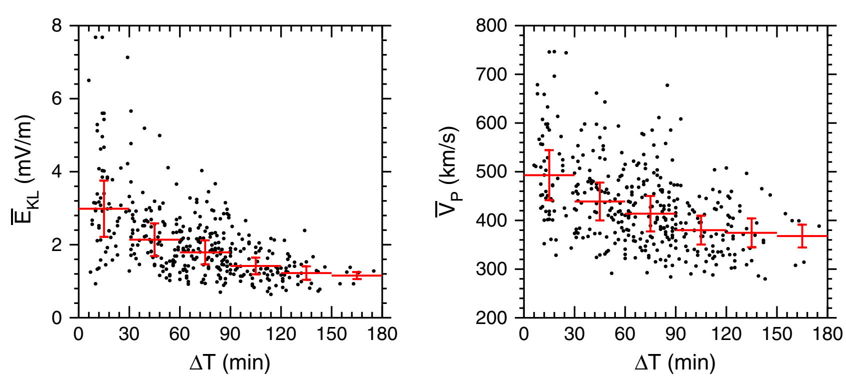

Figure 5. Impacts of solar wind parameters on growth phase duration. (left) The averaged value of solar wind electric field during the growth phase, $\overline{E_{KL}}$; (right) The averaged value of solar wind bulk speed during the growth phase, $\overline{V_P}$. The red horizontal lines represent the geometric means of $\overline{E_{KL}}$ and $\overline{V_P}$ for every ΔT interval of 30 min. The vertical red lines represent the data variations, $\pm$ 0.5 σ (standard deviation).

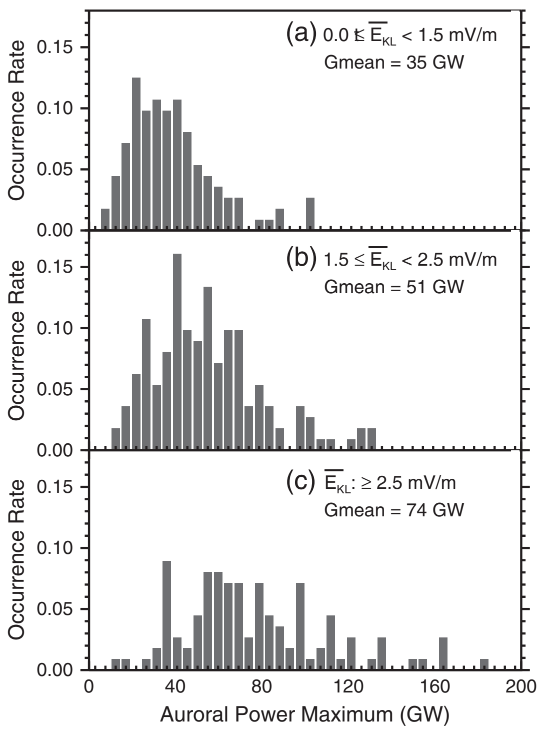

Figure 6. Histogram distribution of auroral power maximum for every 5 GW. (a–c)The three groups mentioned in section 3.3. The vertical coordinate represents the occurrence rate.

wind bulk speed during the growth phase, $\overline{V_P}$. An obvious trend is that the duration of growth phase gets longer as the $\overline{E_{KL}}$ and $\overline{V_P}$ decrease, especially for ΔT less than 120 min. However, for ΔT greater than 120 min, the $\overline{E_{KL}}$ and $\overline{V_P}$ are kept nearly unchanged at 1.2 mV/m and 370 km/s as ΔT increases, suggesting that there must be some thresholds for substorm occurrence. Note that the minimum thresholds of $\overline{E_{KL}}$ and $\overline{V_P}$ are about 0.6 mV/m and 280 km/s, respectively.

3.5. Substorm Intensity

[28] The histogram distribution of auroral power maximum for every 5 GW is shown in Figure 6. The auroral power maximum obviously moves rightward as the $\overline{E_{KL}}$ increases. For the group of $0.0 \le \overline{E_{KL}} < 1.5$ mV/m, the auroral power maximum ranges mainly from 10 to 110 GW, peaking at 25 GW. The geometric mean is 35 GW. For the group of $1.5 \le \overline{E_{KL}} < 2.5$ mV/m, the auroral power maximum ranges mainly from 15 to 150 GW, peaking at 45 GW. The geometric mean increases to 51 GW. For the group of $\overline{E_{KL}} \ge 2.5$ mV/m, the auroral power maximum ranges mainly from 15 to 190 GW, peaking at 60 GW. The geometric mean is 74 GW. This property is in accord with the results from the superposed epoch analysis of AL index for these three groups.

[29] Figure 7 shows the impact of solar wind parameters on the substorm intensity. (left) The averaged value of solar wind electric field during the growth phase, $\overline{E_{KL}}$; (right) The integration of solar wind electric field during the growth phase, ΣE_{KL}. The correlation coefficient between the auroral power maximum and $\overline{E_{KL}}$ and ΣE_{KL} are 0.64 and 0.04, respectively.

[30] To test the goodness of linear correlation coefficients, a Monte Carlo resampling method is employed to determine the 95% significance level of the correlation coefficient threshold. If the correlation coefficient is significantly greater than the threshold value, it represents that there may be a linear correlation between these two parameters; and if the correlation coefficient is significantly less than the threshold value, it means that these two parameters are likely to be independent. Of course, the correlation coefficient is not the sole criteria to judge whether there is a linear correlation between the two parameters. The detailed data distribution is also very important, especially when the correlation coefficient is not quite close to 1 or –1.

[31] The calculated threshold value is 0.09. Thus, it is clear that there is a linear correlation between the auroral power maximum and $\overline{E_{KL}}$ (with correlation coefficient of $0.64 \gg$ the threshold value of 0.09 and the approximate linear data distribution). However, the auroral power maximum is likely to be independent from the integration

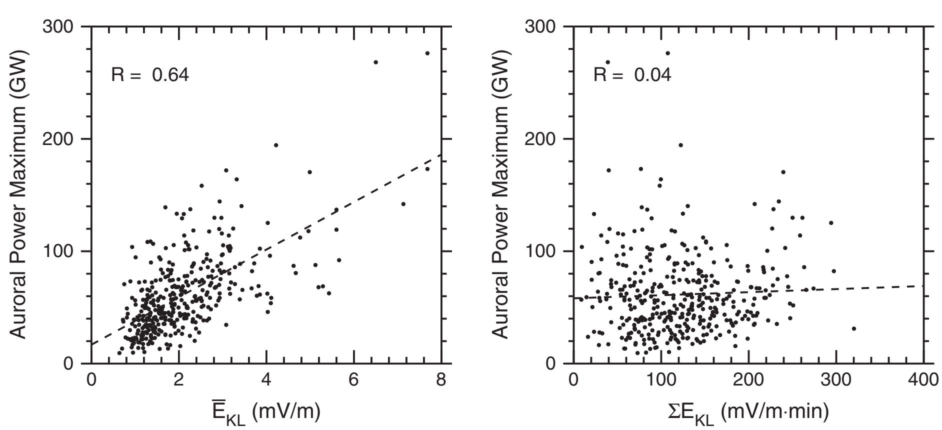

Figure 7. Impacts of solar wind parameters on auroral power maximum. (left) The averaged value of solar wind electric field during the growth phase, $\overline{E_{KL}}$; (right) The integration of solar wind electric field during the growth phase, ΣE_{KL}. The dashed line represents the linear fitting. And R is the linear correlation coefficient.

Table 1. Correlation Coefficients Between Solar Wind Parameters and Auroral Power Maximum During a Substorm, for Both the Average Values and Integrations During Substorm Growth Phase

	Average	Integration
E_{KL}	0.64	0.04
$\mathrm{d}\Phi/\mathrm{d}t$	0.55	0.00
ε	0.50	0.24
IMF B_Z	–0.35	0.03
V_P	0.38	–0.25

of solar wind electric field (with correlation coefficient of 0.04 $\ll$ the threshold value of 0.09). This implies that the substorm intensity is correlated to the dayside reconnection rate, but not the total magnetic flux, which is converted from closed field to open field by magnetic reconnection.

[32] Meanwhile, some other solar wind parameters, such as IMF B_Z, solar wind speed V_P, solar wind energy transporting power into the magnetosphere (ε function, proposed by *Perreault and Akasofu* [1978]), and the rate magnetic flux is opened at the magnetopause ($\mathrm{d}\Phi/\mathrm{d}t$, proposed by *Newell et al.* [2007]), are also evaluated to investigate their relationships to the substorm intensity. The correlation coefficients are listed in Table 1, for both the average values and their integrations during the growth phase. Similarly, the substorm intensity is linearly correlated to the averages of ε and $\mathrm{d}\Phi/\mathrm{d}t$ (the linear correlation coefficients are 0.50 and 0.55, a little lower than the result of E_{KL}), but not their integrations during the substorm growth phase. The linear relationships of IMF B_Z and solar wind speed V_P to auroral power maximum are much weak, with the linear correlation coefficients of only –0.35 and 0.38.

4. Discussion

[33] The growth phase duration has been shown to last for some tens of minutes by many investigations. A brief comparison is shown in Table 2. *Foster et al.* [1971] presented an averaged picture developed from the features of 54 substorms, finding that the average of growth phase duration was about 80 min. Subsequently, *Iijima and Nagata* [1972], *Caan et al.* [1977], and *Iyemori* [1980] separately studied about 20 substorms, suggesting that the growth phase duration ranges from 22 to 164 min with an average of 75 min. *Kamide and Kokubun* [1996] performed a superposed epoch analysis for 20 large isolated substorms, and argued that the average of growth phase duration was only 40 min, much less than the previous results. By surveying extreme large number of cases from 1995 to 2011 (379 events, about 1 order of magnitude larger than those used in most of the previous studies), we performed the most comprehensive statistical study of growth phase duration. The growth phase duration ranges from 6 to 175 min, with an average of 70 min. As we pointed out previously, the error of growth phase duration is on the order of several minutes. This error is acceptable and still reliable for the statistical investigation, however, it is significant for the events with extremely short duration growth phases. For the event with 6 min growth phase, the true duration is about 12 min by using the expansion onset determined by *Frey et al.* [2004] from IMAGE-FUV. Physically, the magnetosphere needs to propagate information from dayside to nightside, either via magnetospheric convection, Allen wave propagation, or development of the ionospheric convection pattern. The periods of these processes are all on the order of tens of minutes. However, by considering that the error of growth phase duration is on the order of several minutes, our result is basically consistent with previous works.

[34] Besides, much more detailed relationships between growth phase duration and solar wind parameters are investigated here. The growth phase duration is controlled by solar wind conditions. The linear correlation coefficients between growth phase duration and $\overline{E_{\mathrm{KL}}}$ and $\overline{V_P}$ are –0.57 and –0.47, respectively. However, the control factor of growth phase duration is very complicated. Neither the reconnection E-field nor the solar wind bulk speed is the sole contributor. Thus, there appear some uncertainties in the plot of Figure 5. Nevertheless, an obvious trend is that the larger the solar wind E-field and the bulk speed are, the shorter the growth phase will be, especially for the case of ΔT less than 120 min. This is physically understandable. The growth phase is the energy-restoring phase of a substorm. Excess electromagnetic energy from solar wind accumulate in magnetotail during this phase. The solar wind reconnection E-field represents the dayside magnetic reconnection rate, reflecting how fast the dayside closed geomagnetic field is converted to the open magnetic flux. The larger the reconnection E-field is, the faster the dayside geomagnetic field is converted to the open flux. The solar wind bulk speed not only contributes to the magnetic reconnection rate but also controls the time delay of transporting the open magnetic flux to the magnetotail. The larger the bulk speed is, the shorter the time delay is. For the case of ΔT greater than 120 min, the $\overline{E_{\mathrm{KL}}}$ and $\overline{V_P}$ are kept nearly unchanged. It suggests that there exists corresponding thresholds for substorm occurrence.

[35] To quantitatively measure the substorm intensity, the auroral power maximum during a substorm is used in this study. In fact, the situations for AL index minimum, AE index maximum, and auroral power maximum from the auroral precipitation model based on DMSP data [e.g., *Newell et al.*, 2009, 2010] are also investigated, but not shown here. The results are all similar. These proxy parameters of substorm intensity are positively correlated to the average of solar wind reconnection E-field during growth phase, but not to the total amount of geomagnetic flux converted to open flux. *Tanskanen et al.* [2005] proposed that the solar wind high-speed streams strongly modulate the substorm intensity in terms of ionospheric dissipation by

Table 2. Comparison of Growth Phase Duration Gained by Several Studies

Author	Case Number	Range (min)	Average (min)
Foster et al. [1971]	54	—	80
Iijima and Nagata [1972]	18	60 ~ 120	—
Caan et al. [1977]	18	22 ~ 164	88
Iyemori [1980]	21	40 ~ 91	63
Kamide and Kokubun [1996]	20	—	40
This work	379	6[a] ~ 175	70

[a]The error is on the order of several minutes. The true duration for this event is about 12 min by using the expansion onset determined by *Frey et al.* [2004] from IMAGE-FUV.

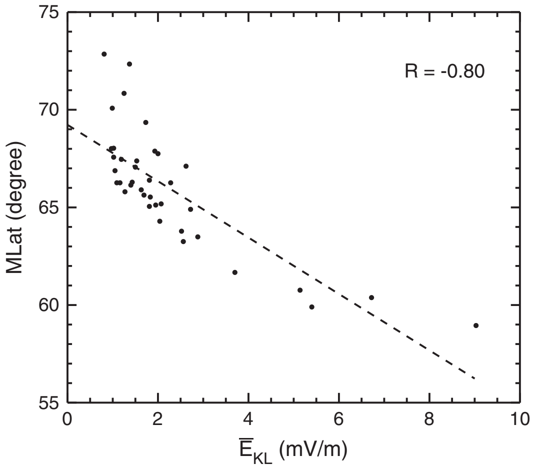

Figure 8. Relationship between the geomagnetic latitude of substorm onset and the averaged value of solar wind electric field during the growth phase, $\overline{E_{KL}}$. The dashed line represents the linear fitting result. R is the correlation coefficient.

Joule heating and auroral electron precipitation. Our result also gives a positive relationship between solar wind speed and auroral power maximum, which is consistent with the conclusion of *Tanskanen et al.* [2005].

[36] In addition, *Milan et al.* [2009] used the auroral brightness from IMAGE to represent the substorm intensity and found that the substorm intensity is larger when the onset latitude is lower. Similarly, *Peng et al.* [2013] also argued that the substorm intensity in terms of both the decrease of AL index and the total intensity of the auroral bulge is inversely correlated with substorm onset latitude. The magnetic latitudes of substorm onsets are found to be correlated with some solar wind parameters, such as solar wind dynamic pressure and IMF B intensity [*Gérard et al.*, 2004]. The onset latitude decreases with increasingly dynamic pressure and IMF B intensity. Based on the 42 identified IMF southward turning events in subsection 2.2, we studied the relationship between the geomagnetic latitude of substorm onset (MLat) and the averaged value of solar wind electric field during the growth phase, $\overline{E_{KL}}$. The Malt is determined by *Frey et al.* [2004] from Far Ultraviolet Imaged (FUV) on board the IMAGE satellite. In Figure 8, it is clear that the substorm onset latitude is negatively correlated to $\overline{E_{KL}}$, with the correlation coefficient of –0.80. Thus, the substorm intensity increases when $\overline{E_{KL}}$ enhances. And our result is also in agreement with the conclusions of *Milan et al.* [2009].

5. Summary

[37] A comprehensive statistical survey of IMF southward turning events is performed to study the impacts of solar wind conditions on substorms, focusing on the following two important questions in substorm study: (1) solar wind impacts on growth phase duration; and (2) solar wind impacts on substorm intensity. A total of 379 IMF southward turning events from 1995 to 2011 are identified. The statistical study of large number of cases is very necessary and of great importance to obtain a more detailed understanding on this issue. The main results are remarked as follows:

[38] 1. The growth phase persists from several minutes to about 3 h, which is controlled by the solar wind conditions. The larger the dayside reconnection rate and the solar wind speed are, the shorter the growth phase duration will be. However, there are some lower limits of solar wind reconnection E-field and bulk speed for substorm occurrence. The thresholds are 0.6 mV/m and 280 km/s, respectively.

[39] 2. The substorm intensity is linearly correlated to the dayside reconnection rate. However, it seems to be independent of the amount of dayside geomagnetic flux converted to open flux during the growth phase. Similar results are obtained for other solar wind parameters, such as the solar wind energy transporting power into the magnetosphere (ε function, proposed by *Perreault and Akasofu* [1978]) and the rate of magnetic flux is opened at the magnetopause ($d\Phi/dt$, proposed by *Newell et al.* [2007]).

[40] 3. Superposed epoch analysis is performed to show further and detailed verification. All the events are divided into three groups with different $\overline{E_{KL}}$ during the growth phase: (1) $0.0 \leq \overline{E_{KL}} < 1.5$ mV/m; (2) $1.5 \leq \overline{E_{KL}} < 2.5$ mV/m; and (3) $\overline{E_{KL}} \geq 2.5$ mV/m. The geometric means of growth phase duration and auroral power maximum for these three groups are 91 min, 62 min, 32 min, and 35 GW, 51 GW, 74 GW, respectively.

[41] **Acknowledgments.** We thank J. R. Kan for very helpful discussions. The OMNI data were obtained from the GSFC/SPDF OMNIWeb interface at *http://omniweb.gsfc.nasa.gov*. The hemispheric auroral power data provided by NOAA/POES were obtained from the website at *http://www.swpc.noaa.gov/ftpdir/lists/hpi*. This work was supported by 973 program 2012CB825602, NNSFC grants 41204118 and 41231067, and in part by the Specialized Research Fund for State Key Laboratories of China.

[42] Masaki Fujimoto thanks Tohru Araki and another reviewer for their assistance in evaluating this paper.

References

Akasofu, S. I. (1964), The development of the auroral substorm, *Planet. Space. Sci.*, *12*, 273.

Akasofu, S. I., S. Chapman, and C. I. Meng (1966), The polar electrojet, *J. Atmos. Terr. Phys.*, *30*, 227.

Baker, D. N. (1996), Solar wind-magnetosphere drivers of space weather, *J. Atmos. Terr. Phys.*, *58*, 14.

Baker, D. N., S. I. Akasofu, W. Baumjohann, J. W. Bieber, D. H. Fairfield, E. W. Hones Jr., B. Mauk, R. L. McPherron, and T. E. Moore (1984), Substorms in the magnetosphere, in *Solar Terrestrial Physics-Present and Future*, edited by D. M. Butler and K. Papadopoulos, NASA Ref. Publ., 1120, chap 8.

Caan, M. N., R. L. Mcpherron, and C. T. Russell (1977), Characteristics of the association between the interplanetary magnetic field and substorms, *J. Geophys. Res.*, *82*, 4837–4842.

Cowley, S. W. H., and M. Lockwood (1992), Excitation and decay of solar wind-driven flows in the magnetosphere-ionosphere system, *Ann. Geophys.*, *10*, 103.

Dmitrieva, N. P., and V. A. Sergeev (1983), Spontaneous and triggered onsets of substorm expansion and duration of the substorm growth phase, *Geomagn. Aeron. (in Russian)*, *23*, 474.

Dmitrieva, N. P., and V. A. Sergeev (1985), Duration of the preliminary phase of substorms with a spontaneous burst commencement, *Geomagn. Aeron. (in Russian)*, *25*, 425–427.

Foster, J. C., D. H. Fairfield, K. W. Oglivie, and T. J. Rosenberg (1971), Relationship of interplanetary parameters and occurrence of magnetospheric substorms, *J. Geophys. Res.*, *76*, 6971–6975.

Frey, H. U., S. B. Mende, V. Angelopoulos, and E. F. Donovan (2004), Substorm onset observations by IMAGE-FUV, *J. Geophys. Res.*, *109*, A10304, doi:10.1029/2004JA010607.

Gérard, J. C., B. Hubert, A. Grard, M. Meurant, and S. B. Mende (2004), Solar wind control of auroral substorm onset locations observed with the IMAGE-FUV imagers, *J. Geophys. Res.*, *109*, A03208, doi:10.1029/2003JA010129.

Gjerloev, J. W., R. A. Hoffman, E. Tanskanen, M. Friel, L. A. Frank, and J. B. Sigwarth (2003), Auroral electrojet configuration during substorm growth phase, *Geophys. Res. Lett.*, *30*(18), 1927, doi:10.1029/2003GL017851.

Hsu, T. S., and R. L. McPherron (1996), Occurrence frequency of substorm field and plasma signatures observed near-earth by ISEE-1/2, in *Proceedings of Third International Conference on Substorms (ICS-3)*, edited by E. J. Rolfe, and B. Kaldeich, 333-C340, Eur. Space Agency, Versailles, France.

Hsu, T. S., and R. L. McPherron (1998), The main onset of a magnetospheric substorm, in *Proceedings of Fourth International Conference on Substorms (ICS-4)*, edited by S. Kokubun, and Y. Kamide, 79C-82, Terra Sci., Tokyo.

Iijima, T., and T. Nagata (1972), Signatures for substorm development of the growth and expansion phase, *Planet. Space Sci.*, *20*, 1095.

Iyemori, T. (1980), Time Delay of the substorm onset from the IMF southward turning, *J. Geomag. Geoelectr.*, *32*, 267–273.

Kan, J. R., and L. C. Lee (1979), Energy coupling function and solar wind-magnetosphere dynamo, *Geophys. Res. Lett.*, *6*(7), 577–580.

Kamide, Y., and N. Fukushima (1972), Positive geomagnetic bays in evening high-latitudes and their possible connection with partial ring current, *Rep. Ionos. Space Res. Japan*, *26*, 79.

Kamide, Y., P. D. Perreault, S. I. Akasofu, and J. D. Winningham (1977), Dependence of substorm occurrence probability on the interplanetary magnetic field and on the size of the auroral oval, *J. Geophys. Res.*, *82*, 5521–5528.

Kamide, Y., and J. F. Vickrey (1983), Variability of the Harang discontinuity as observed by the Chatanika radar and the IMS Alaska magnetic chain, *Geophys. Res. Lett.*, *10*, 159ÍC-162.

Kamide, Y., and S. Kokubun (1996), Two-component auroral electrojet: Importance for substorm studies, *J. Geophys. Res.*, *101*, 13, 027.

Lui, A. T. Y. (1993), What determines the intensity of magnetospheric substorms? *J. Atmosph. Terr. Phys.*, *55*(8), 1123–1136.

McPherron, R. L. (1970), Growth phase of magnetospheric substorms, *J. Geophys. Res.*, *75*, 5592.

McPherron, R. L. (1994), The growth phase of magnetospheric substorms, in *Proc. Second International Conference on Substorms (ICS-2)*, edited by J. R. Kan, J. D. Craven, and S. I. Akasofu, pp. 213–220, Geophysical Institute, University of Alaska, Fairbanks.

Meng, C. I., B. Tsurutani, K. Kawasaki, and S. I. Akasofu (1973), Cross-correlation analysis of the AE index and the interplanetary magnetic field Bz component, *J. Geophys. Res.*, *78*, 617–629.

Milan, S. E., A. Grocott, C. Forsyth, S. M. Imber, P. D. Boakes, and B. Hubert (2009), A superposed epoch analysis of auroral evolution during substorm growth, onset and recovery: open magnetic flux control of substorm intensity, *Ann. Geophys.*, *27*, 659 C-668.

Newell, P. T., T. Sotirelis, K. Liou, C. I. Meng, and F. J. Rich (2007), A nearly universal solar wind-magnetosphere coupling function inferred from 10 magnetospheric state variables, *J. Geophys. Res.*, *112*, A01206, doi:10.1029/2006JA012015.

Newell, P. T., T. Sotirelis, and S. Wing (2009), Diffuse, monoenergetic, and broadband aurora: The global precipitation budget, *J. Geophys. Res.*, *114*, A09207, doi:10.1029/2009JA014326.

Newell, P. T., T. Sotirelis, and S. Wing (2010), Seasonal variations in diffuse, monoenergetic, and broadband aurora, *J. Geophys. Res.*, *115*, A03216, doi:10.1029/2009JA014805.

Peng, Z., C. Wang, Y. F. Yang, H. Li, Y. Q. Hu, and J. Du (2013), Substorms under northward interplanetary magnetic field: Statistical study, *J. Geophys. Res. Space Physics*, *118*, 364–374, doi:10.1029/2012JA018065.

Perreault, P., and S. I. Akasofu (1978), A study of geomagnetic storms, *Geophys. J. R. Astron. Soc.*, *54*, 547–573.

Petrukovich, A. A. (2000), The growth phase: Comparison of small and large substorms, in *Proc. 5th International Conference on Substorms (ICS-5)*, edited by A. Wilson, pp. 9–14, European Space Agency, St. Petersburg, Russia.

Ridley, A. J., G. Lu, C. R. Clauer, and V. O. Papitashvili (1997), Ionospheric convection during nonsteady interplanetary conditions, *J. Geophys. Res.*, *102*(14), 564.

Ridley, A. J., G. Lu, C. R. Clauer, and V. O. Papitashvili (1998), A statistical study of the ionospheric convection response to changing interplanetary conditions using the assimilative mapping of ionospheric electrodynamics technique, *J. Geophys. Res.*, *103*, 4023.

Rostoker, G. (1969), Classification of polar magnetic disturbances, *J. Geophys. Res.*, *74*, 5161.

Rostoker, G., H. L. Lam, and W. D. Hums (1972), Response time of the magnetosphere to the interplanetary electric field, *Can. J. Phys.*, *50*, 544–547.

Ruohoniemi, J. M., and R. A. Greenwald (1998), The response of high-latitude convection to a sudden southward IMF turning, *Geophys. Res. Lett.*, *25*, 2913.

Russell, C. T., and R. L. McPherron (1973), Semiannual variation of geomagnetic activity, *J. Geophys. Res.*, *78*, 92.

Saito, T., T. Sakurai, and Y. Koyama (1976), Mechanism of association between Pi2 pulsation and magnetospheric substorm, *J. Atmos. Terr. Phys.*, *38*, 1265–1277.

Tanskanen, E., T. I. Pulkkinen, H. E. J. Koskinen, and J. A. Slavin (2002), Substorm energy budget during low and high solar activity: 1997 and 1999 compared, *J. Geophys. Res.*, *107*, A6,1086, doi:10.1029/2001JA900153.

Tanskanen, E. I., J. A. Slavin, A. J. Tanskanen, A. Viljanen, T. I. Pulkkinen, H. E. J. Koskinen, A. Pulkkinen, and J. Eastwood (2005), Magnetospheric substorms are strongly modulated by interplanetary high-speed streams, *Geophys. Res. Lett.*, *32*, L16104, doi:10.1029/2005GL023318.